MSA UNIVERSITY ENGINEERING JOURNAL

Numerical and Experimental Investigations of Bladeless Wind Turbine for Green Energy Applications

Khaled Nagdy Faris[a,b], Abdelrahman Naiem[a], Sara Hesham[a], and Mohammed Ali Abdelnaby [a]

[a] Mechatronics Systems Engineering Department, October University for Modern Sciences and Arts-MSA, Giza, Egypt
[b] Power Electronics and Energy Conversion Department, Electronics Research Institute, Cairo-Egypt.

E-mail: knfaris@msa.edu.eg (Corresponding author)

Abstract:
Green energy applications have been a promising research area last two decades. One of these applications is using the power of wind for electrical power generation; wind turbines with different designs have great importance in this field. However, capturing energy from wind by using traditional wind farms has several limitations such as large installation space, specified airflow conditions, shading effect, noise, and design and maintenance complexity. Bladeless wind turbines have been used to convert wind energy into useful kinetic energy to overcome these obstacles. This paper introduces numerical and experimental investigations of a bladeless wind turbine for harvesting energy from wind. The proposed design has a cylindrical structure to resonate at a wide range of wind speeds and directions, which can maximize the harvested energy. Eigen-frequency simulation modules were developed to determine the structure's natural frequencies and mode shapes which aimed for continuous tunning with the generated vortex shed frequency. Furthermore, the numerical investigations extended to simulate the fluid-structure interaction (FSI) analysis to accurately define the dynamic response of the bladeless wind turbine under different air-flow conditions. The resulting kinetic energy is delivered to an alternator to convert it into electrical power.

Keywords: Energy harvesting -Bladeless wind turbine - Electro aero-elastic models

1. Introduction

Bladeless wind turbines are a new approach to harnessing wind power and converting it to electricity [1 and 2]. Vortex shed techniques don't use blades; simply, it uses an oscillatory motion to harvest power from the wind without the need to use a lot of mechanical lumped elements such as brakes, gears, pitch, yaw, and lubricants. Furthermore, bladeless wind turbines are characterized by simple design, environmental friendliness, on-site production, and low initial cost [3]. Many bluff body shapes were used in the fluid-structure interaction analysis using a circular cross-section is preferred because it has a good performance in initiating vortex shed frequency at a wide bandwidth of fluid flow conditions [4].
Much research discussed the Fluid-Structure Interaction (FSI) for enhancing kinetic energy gained [5 and 6] the biggest challenge is using the cross section which has outstanding performance at different discharge properties [7 and 8]. In the case of using air as a working fluid and focusing on renewable energy applications, capturing wind energy and convert to electricity, in these conditions, there is a certain range of useful wind speeds [9]. After defining the fluid speed now, one can choose a suitable cross-section to maximize lift and drag coefficients by examining the dynamic performance using Computational Fluid Dynamic (CFD) modules [4 and 10].
Electro-aeroelastic problems become the last step to converting captured kinetic energy from the bladeless windmill to electrical energy [11]. Energy conversion techniques from mechanical to electrical have three main classifications: electromagnetic [12 and 13], electrostatic [14], and piezoelectric [15 and 16].

Finally, the bladeless wind turbines have a great significance last few years. The required design and fabrication analysis have been briefly introduced. In this study, the complete design, numerical simulations, manufacturing procedures, and experimental investigations are developed for the cylindrical bladeless wind turbine.
The remainder of this paper is structured into seven sections. Section 2 presents the design of the bladeless wind turbine for extracting mechanical energy. Section 3 presents a time-dependent solid mechanics model to estimate the wind stream's periodic loads. Section 4 presents an alternator simulation. Section 5 discusses the experimental validations. Finally, Section 6&7 is dedicated to the conclusions and recommendations.

2. Bladeless Wind Turbine Design

The components of the proposed bladeless wind turbine are depicted schematically in "Figure 1." The windmill's mast and cantilever beam, which carry it, are its primary components. Because of its low weight and high strength, fiberglass was selected as the material for the mast, and carbon fibre was used to manufacture the cantilever beam. The windmill's vibration pattern is caused when the wind stream comes into contact with the mast, which has a cylinder shape.

This causes a vortex shed, which creates different pressures in the areas behind the mast. An alternator was used to convert the gathered kinetic energy into usable electrical energy.

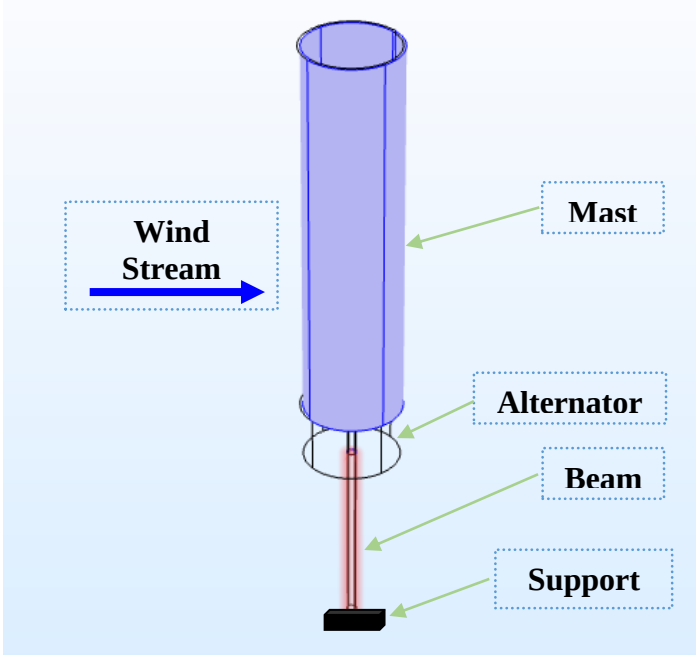

Fig. 1 Schematic illustration for the bladeless wind turbine

There are three studies for the phases of analysis: First, a fluid-structure interaction module to determine the selected bluff body's "circular section" lift and drag coefficients; second: extracted Fluid-Structure Interaction (FSI) forces so that they could influence the mast's external boundary. The reaction forces at the cantilever tip can then be determined, and finally: electromechanical analysis to replicate the electrical energy.

2.1. Fluid-Structure Interaction

Figure 2 shows the circular section under wind stream effects with constant air velocity U, which has three different values in this study 4, 7, and 10 m/s; these values were chosen to simulate the wind speed ranges in Egypt [9]. According to Eq. (1), Reynold's number is 10^5, 1.7×10^5, and 2.4×10^5.

$$Re = UD/\nu \quad (1)$$

Where: U is an air linear velocity [m/s], D characteristic length (diameter) of a circular section [m], and ν is a kinematic viscosity of air [m^2/s].

The Fluid-Structure Interaction (FSI) model simulated the velocity and pressure distributions around the circular section at 10^5 and 10^6 Reynolds numbers, as shown in Fig. 2. This model has been developed by using COMSOL Multiphysics software.

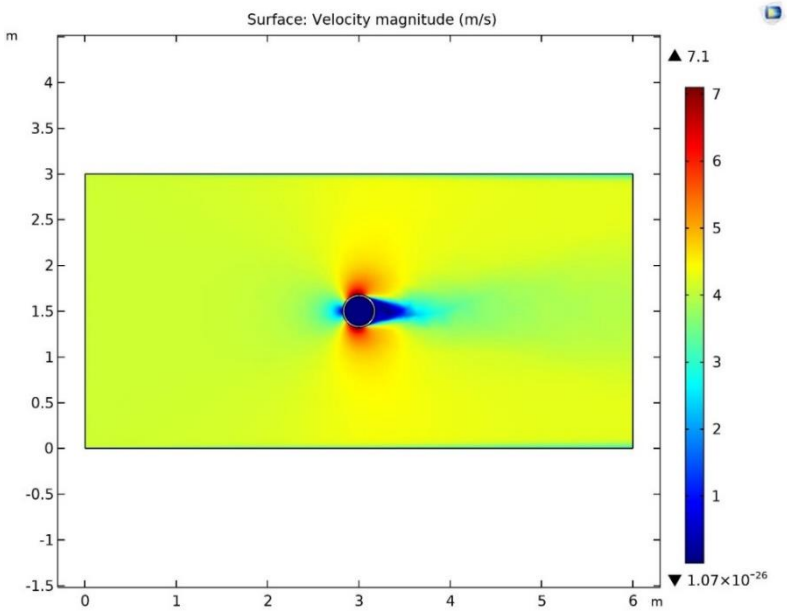

(a) Velocity profile at U = 4 m/s and Re=10^5

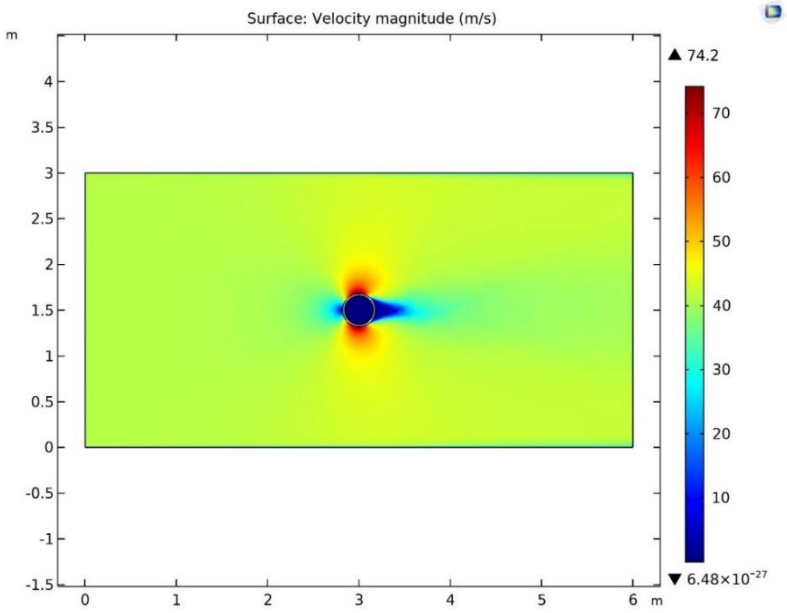

(b) Velocity profile at U = 41 m/s and Re=10^6

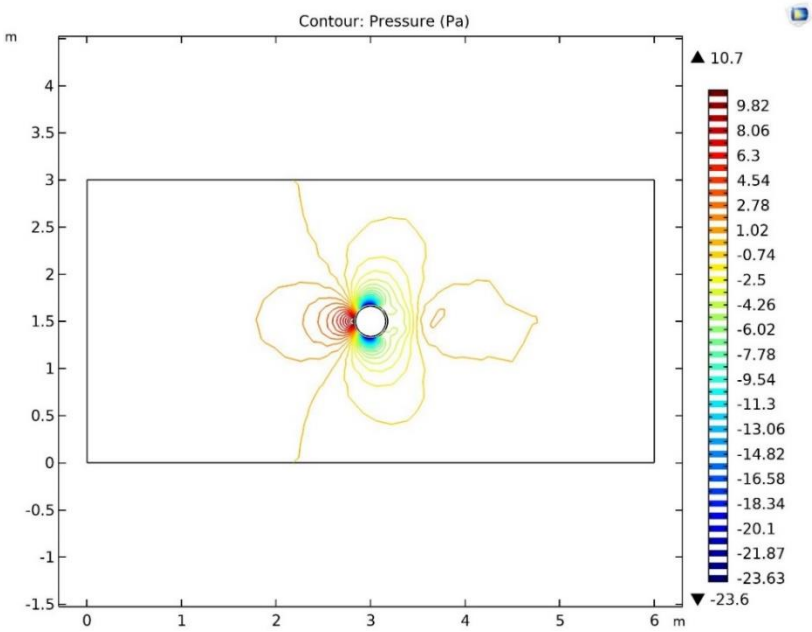

(c) Pressure distribution at U = 4 m/s and Re=10^5

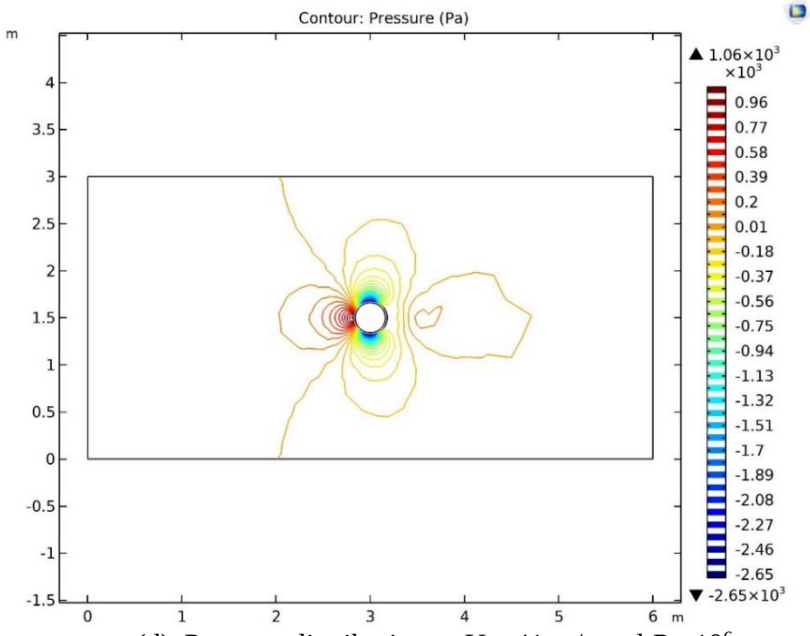

(d) Pressure distribution at U = 41 m/s and R_e=10^6

Fig. 2 Velocity and pressure distribution around the circular section

Some of the output results from the FSI model were obtained at wind velocities of 4 and 41 m/s, all at the circular section with an output diameter equal to 360 mm and an out-of-plane length of 2.75 m. Figure 2 Clearly shows that as the wind speed increases, the velocity and pressure values around the bluff object rise, increasing the mast's kinetic energy.

The prospective study was extended to estimate the total reaction forces in the air stream direction (drag force) and perpendicular to it (lift force). By using the fluid dynamic relations [17] can estimate the drag and lift coefficients as shown in Eq. (2):

$$F_D = 0.5\, C_D \rho D U^2$$
$$F_L = 0.5\, C_L \rho D U^2 \quad (2)$$

Where ρ is air density at atmospheric pressure kg/m^3], C_D&C_L drag and lift coefficients, respectively.

The Computational Fluid Dynamic (CFD) model which was created to estimate the lift and drag reactions of a circular section under certain fluid dynamic conditions has been divided into two sections, first; turbulence fluid analysis where its output stresses be a given input to a solid mechanics module to calculate the force of reactions in x and y directions (Drag and Lift components, respectively). The numerical data estimated have been compared with previous studies as shown in Table 1.

Table 1. Benchmarked analysis for Computational Fluid Dynamic (CFD) model

	Drag Coefficient C_D		**Lift Coefficient C_L**	
	Re=10^5	**Re=10^6**	**Re=10^5**	**Re=10^6**
Fundamentals of Fluid Mechanics, (Bruce R. Munson, 2009) [17]	1.15	0.777		
Developed Numerical Model (Jiyuan Tu, 2018) [4]	1.19	0.882		
			<0.1	<0.1
Developed Numerical Model			0.027	0.00348

It's clear from the results in Table 1 the convergence of the values of drag and lift coefficients in the recent study and previous ones.

2.2. Eigen-frequency analysis

It's important to understand the dynamic performance of the bladeless windmill by studying the Eigen frequency windmill modules as shown in the following two sections.

2.2.1. Vortex shedding frequency.

Now the study was directed to estimate the total reaction forces in drag and lift directions (R_x and R_y, respectively) at the base of the mast. These forces are generated by the effect of the wind stream on the mast which was investigated in section 2.1. For completing viewing the whole problem under analysis, the vortex shedding, and a Kármán vortex street must be defined.

Vortex shedding is an oscillating flow pattern in fluid dynamics theorems that occurs when a certain fluid, flows past a bluff body at a specific Reynolds number, depending on the body's shape and dimensions. A Kármán vortex street is formed when vortices patterns form behind the body and periodically separate from either side of the body in this flow. On the object's downstream side, the fluid flow creates an alternating low-pressure region in which the bluff body will likely move and instantaneously stable. So, the bladeless windmill structure is designed to have natural frequencies that match the vortex shedding frequencies to harvest maximum kinetic energy at resonance states also, taking into consideration the maximum allowable stresses according to the design selected materials.

As a selected mast's cross-sectional shape is cylindrical, the following Eq. (3) relates the Strouhal number to the frequency of vortex shedding for an infinite cylinder [17].

$$S_t = fD/U \tag{3}$$

Where f is the frequency of vortex shedding [r/s], D is the characteristic length of the bluff body (cylinder diameter in this study) [m], U is the linear air velocity [m/s], and St is the dimensionless Strouhal number, which equals 0.22 in the cylindrical shape at a wide range of Reynolds number.

According to the resonance constraints and desired tunning system with the vortex shedding frequency, the parameters of a proposed bladeless windmill and its components are viewed in Table 2.

Table 2. Material and dimensions of the proposed bladeless windmill

Components	**Material**	**Length [m]**	**Diameter [mm]**
Mast	Fiberglass	2.75	Outer 360 & Inner 320
Cantilever Beam	Carbon fibre	1.3	Outer 35 & Inner 33

2.2.2. Bladeless windmill mode shapes

Using the data given in Table 2, the eigenfrequency model has been devolved to investigate the natural frequencies and their normal modes as shown in Figure 3.

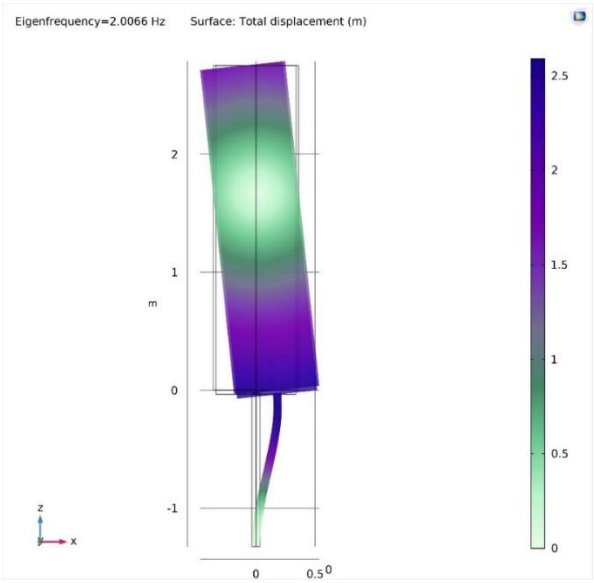

(a) First mode shape of the bladeless windmill, $\omega_n = 4\pi\, s^{-1}$

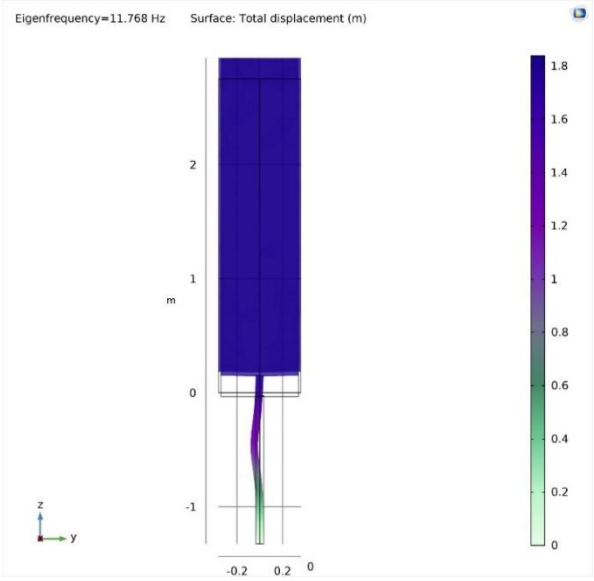

(b) Second mode shape of the bladeless windmill, $\omega_n = 23.5\pi\, s^{-1}$

Fig. 3 Natural frequencies and normal modes for the bladeless windmill

As shown in Fig. 3, the fundamental natural frequency equals 2 Hz for the proposed design of the bladeless windmill.

In the case of vortex shedding flows with a frequency close to the fundamental natural frequency, the resonance phenomenon grows, and the windmill

experiences maximum deformations. In these situations, the stresses must still be less than the maximum allowable stresses based on the yield strength of carbon fibre, as shown in Fig 4.

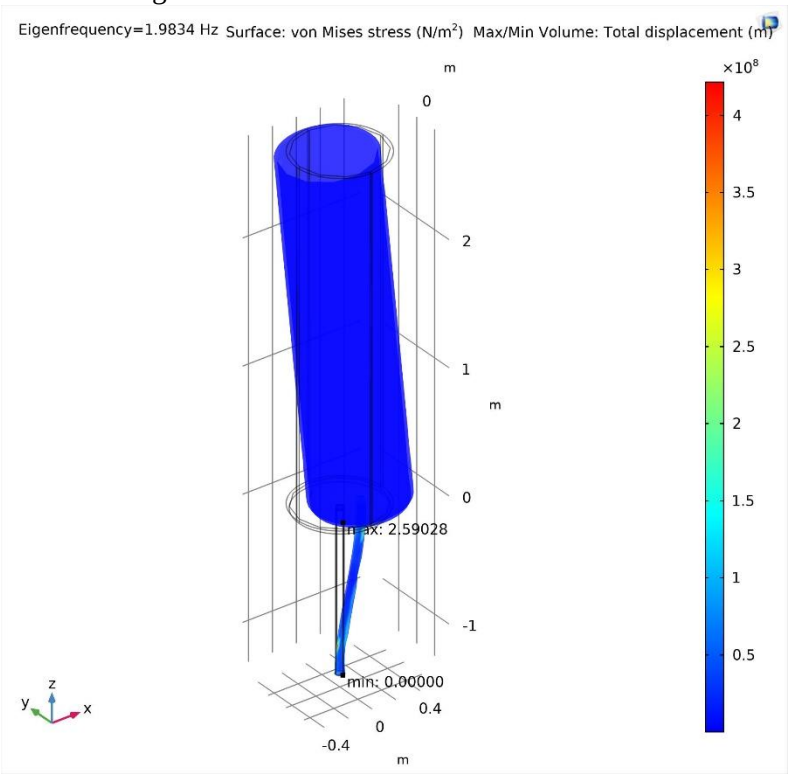

Fig.4 Maximum/Minimum von Mises stress and total displacement at the fundamental natural frequency

It is clear from Fig. 4, that the maximum stresses do not exceed 260×10^{6} Pa which is less than the minimum allowable strength of carbon fibre (800 MPa) [18] and fiberglass (1200 MPa) [19].

3. Solid mechanics model

After the numerical simulation analysis discussed in section 2, the extracted fluid dynamics force now affects the wind turbine structure and produces the desired oscillatory motions. This section covers the numerical solid mechanics model created to simulate the mechanical vibrations of the mast under erratic loads.

Figure 5 shows the bladeless wind turbine under the effect of wind loads, which calculated the computational fluid dynamics module (CFD) (in *x* and *y* directions).

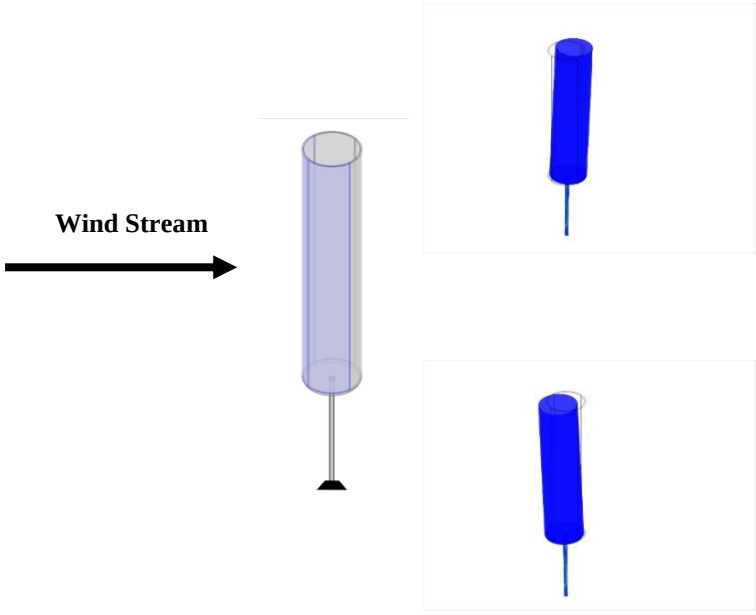

(a) Bladeless wind turbine under dynamic loads

(b) Periodic resulting motions

Fig. 5 Bladeless windmill under aero-dynamic loads

The time-dependent study has been developed by representing the wind loads as sinusoidal forces with amplitudes equal to the magnitudes of drag and lift forces in the x and y directions, respectively. The frequency of those forces was calculated from the vortex shedding analysis discussed previously in section 2.
Three cases have been chosen for the vortex shedding frequency values namely, 2, 4, and 11 Hz. These values cover a good range of wind speed and contain the bladeless wind turbine's first and second natural frequencies under investigation.
Figure 6 shows the total reaction forces at the mast's base or the cantilever beam tip.

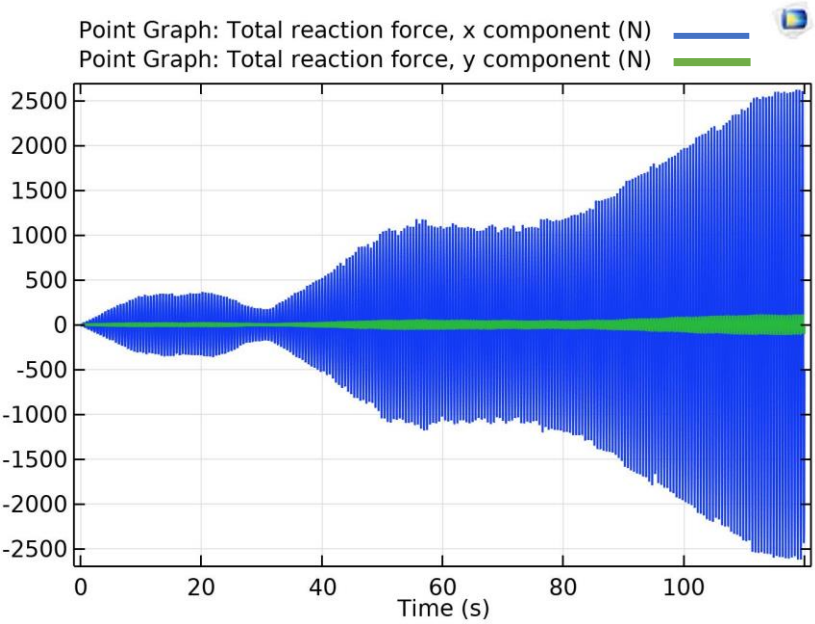

(a) Resonant force response at 2 Hz vortex shedding frequency

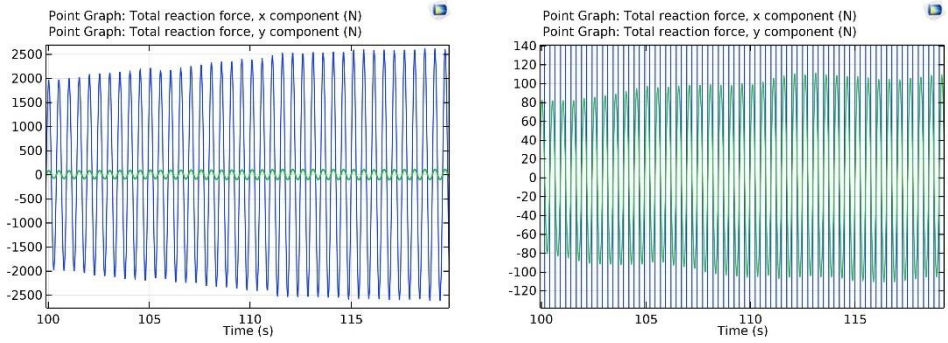

(b) Zoom in the case in part (a) from *t=100 s to t=120 s*

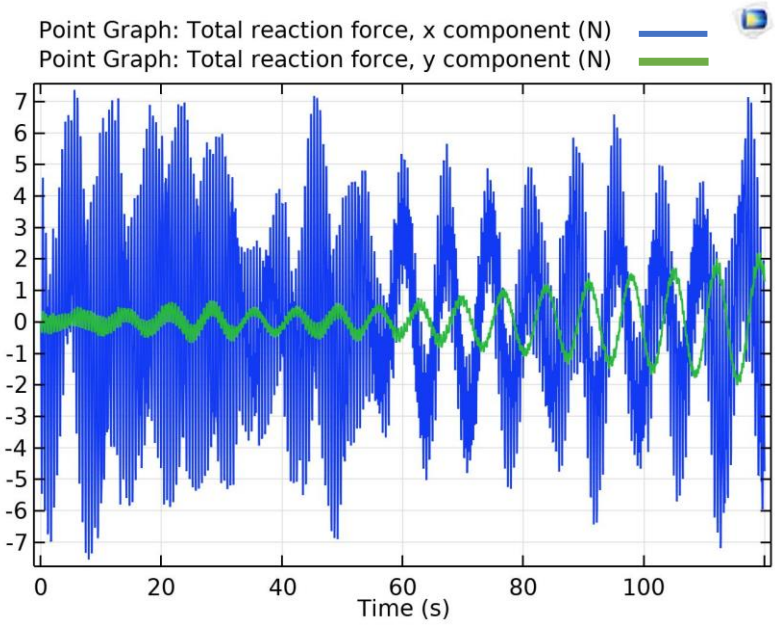

(c) Forec Responses at 4 Hz vortex shedding frequency

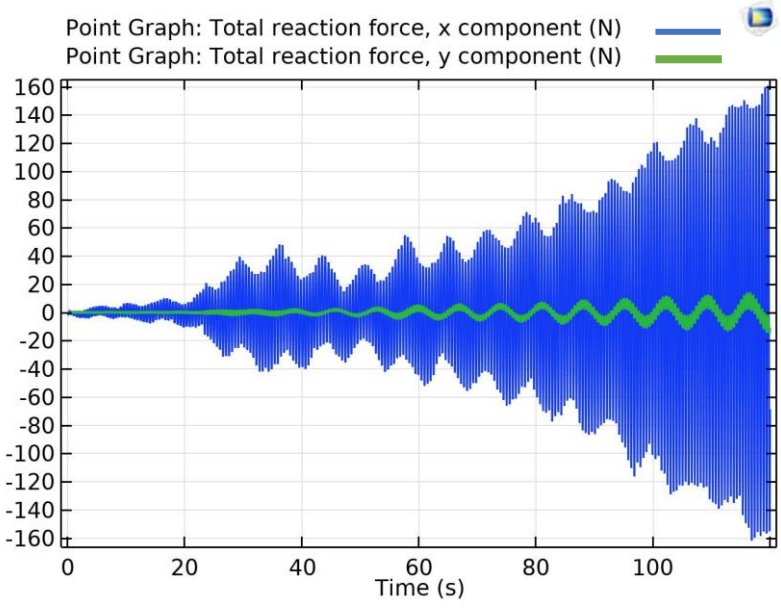

(d) Beating phenomenon at 11 Hz vortex shedding frequency

Fig.6 Reaction forces applied at the cantilever tip at different excited frequencies.

It's clear from Fig. 6 that the applied reaction forces on the beam tip increase when the vortex shedding frequency is close to one of the natural frequencies,

also noted that the drag forces are larger than the lift forces, especially at resonance, which proves the concept of drag machines in bladeless wind turbines.

4. Alternator simulation

The energy conversion from a mechanical to an electrical phase is an important stage in the field of energy harvesting technology and storage. There are many techniques to implement this conversion such as piezoelectric, electrostatic, and electromagnetic. The most popular method is the electromagnetic approach used in this study, as illustrated in [20]. A finite element model for the cantilever employs the Euler-Bernoulli beam theory to investigate the bladeless wind turbine dynamic behaviour. The structure of the vector of nodal degrees of freedom is such that the transverse displacements and angular rotations in the displacement vector, as in Eq. (4)**:**

$$\{z\} = \{z_1 \quad \dot{z}_1 \ldots\ldots\ldots\ldots z_n \quad \dot{z}_n\}^T \tag{4}$$

Where n is the number of degrees of freedom according to the number of elements used.

The formulation that G. Poulin, 2004 [11], had previously developed is extended here to simulate the coupled electro-aeroelastic performance.

G. Poulin, 2004, [11], introduce a forcing term proportional to the induced current, which is proportional to the magnet velocity. The magnets and coils used in this study were mounted at the cantilever beam tip, so the effect of electromagnetic damping as in Eq. (5) will attach at the penultimate node.

$$\{P\} = \{0 \quad 0 \ldots\ldots\ldots\ldots\ldots BL_w \quad 0 \quad 0 \quad 0\} \tag{5}$$

Where B is a magnetic flux density [Tesla]
L_w is wire length [m]

The electro-aeroelastic governing equations for the cantilever beam of the bladeless wind turbine subjected to the FSI reaction forces are as follows,

$$\begin{bmatrix} m & 0 \\ 0 & 0 \end{bmatrix} \begin{Bmatrix} \ddot{z} \\ \ddot{I} \end{Bmatrix} + \begin{bmatrix} c & 0 \\ P & -L_c \end{bmatrix} \begin{Bmatrix} \dot{z} \\ \dot{I} \end{Bmatrix} + \begin{bmatrix} k & P^T \\ 0 & -(R_l + R_c) \end{bmatrix} \begin{Bmatrix} z \\ I \end{Bmatrix} = \begin{Bmatrix} F \\ 0 \end{Bmatrix} \tag{6}$$

Where: m is the equivalent mass matrix [kg], c is the proportional damping according to Inman, 2013, [21], k is the equivalent stiffness matrix [N/m], and L_c [H] and R_c [Ω] is the coil inductance and resistance, respectively. Finally, the force vector will be as follows:

$$\{F\} = \{0 \quad 0 \ldots\ldots\ldots -PI \quad 0 \quad F_A \quad 0\}^T \tag{7}$$

Where F_A: are the aerodynamic loads that result from FSI problems.

Table 3 introduces the required input data for completely solving the electro-aeroelastic model and extracting output voltage and power at various load resistance.

Table 3. electro - aeroelastic problem parameters

Mechanical, Cantilever	Electromagnetic induction	Aerodynamics
Young's Modulus, E = 294 GPa	Magnetic Flux Density, B = 1.6 [Tesla]	Wind speeds. 4, 7, and 10 m/s
Density, ρ = 1820 kg/m^3	Coil wire length L_w = 5 [m]	The equivalent vortex shedding frequencies. 2.44, 4.27, and 6.11 r/s
Outer Diameter, D_o = 70 mm	Coil resistance R_c = 15[Ω]	Equivalent Reynolds number [10, 17, and 24.3]×10^4
Inner Diameter, D_i = 66 mm	Coil inductance L_c = 0.03[H]	Air density = 1.205 kg/m^3
Length = 1.3 m		
Spring Foundation = 600 N/m		
Proportional Damping = 10^{-3} × stiffness matrix		

5. Experimental validation

Figure 7 shows the manufactured components of the bladeless wind turbine. The material, dimensions, and electromagnetic parameters are listed in Tables 2 and 3. As a sample, the experimental open circuit voltage was measured experimentally at 4 Hz vortex shed frequency as shown in Fig. 8. The corresponding numerical output voltage at the same operating condition is shown in Fig. 9. The experimental results look close to the numerical simulations as viewed in Figs. 8 and 9. In order to magnify the gained output voltage, the excitation frequency should be close to one of the natural frequencies of the bladeless wind turbine as shown in Fig. 10.

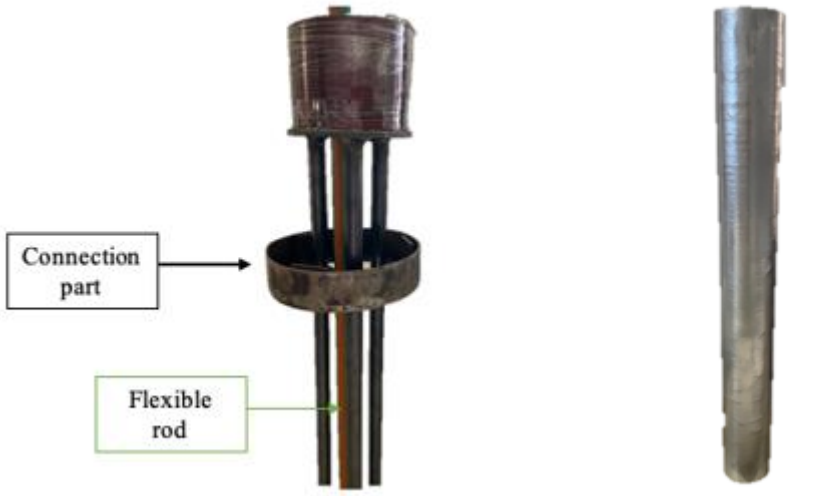

(a) Connection part and the flexible rod (b) Mast

Fig. 7 The main components of the bladeless wind turbine

Figure 7 shows the bladeless wind turbine's main components: (a) the flexible rod with connection part that translate the wind effects to the electromagnetic system and (b) the mast.

Figure 8 shows an experimental result sample of the open circuit voltage harvested from the bladeless wind turbine, while Fig. 9 shows the corresponding numerical open circuit voltage.

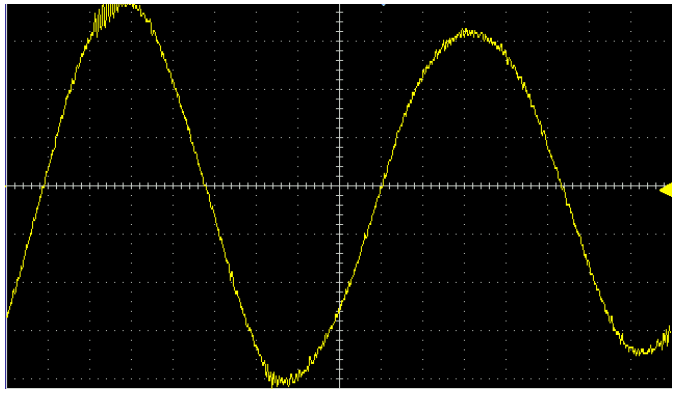

50mv/div

Fig. 8 An experimental result of an output peak voltage (200mV) at 4 Hz vortex shed frequency.

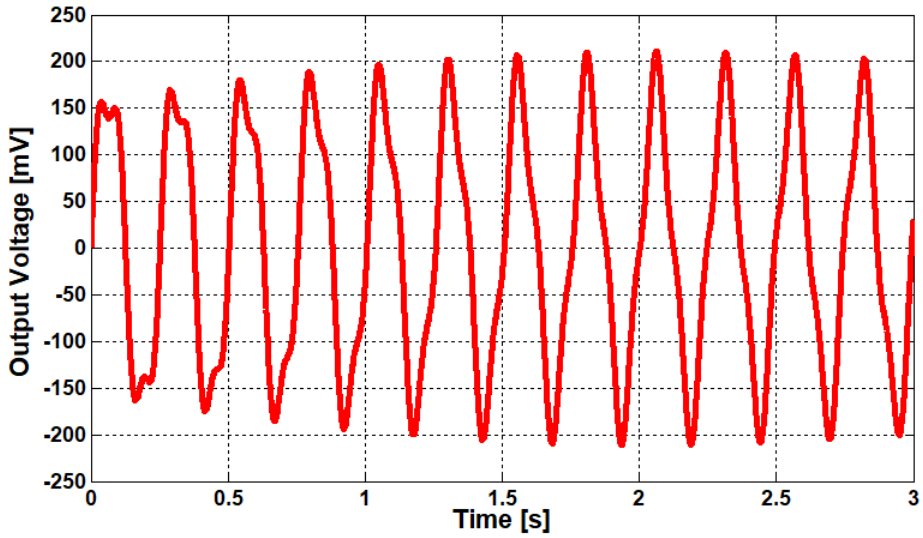

Fig. 9 Numerical time history of the output voltage at 4 Hz vortex shed frequency.

The resonance state for the bladeless wind turbine should have occurred to increase the output voltage to the maximum value. Figure 10 shows the maximum numerical open circuit voltage extracted from the bladeless wind turbine at the second natural frequency which equals 11.7 Hz.

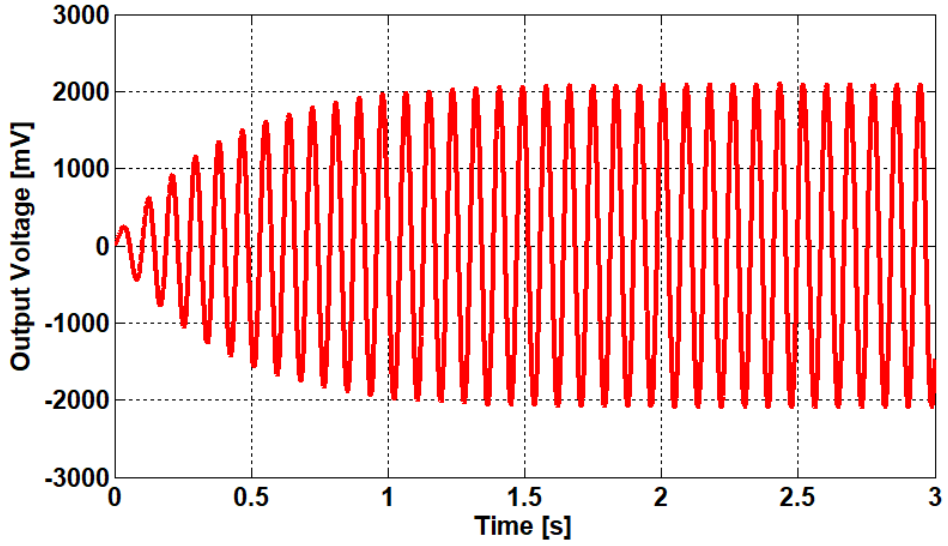

Fig. 10 The numerical time history plot of the output voltage at 11.7 Hz vortex shed frequency.

It's clear from Fig. 10 that the time required to build and stabilize the output voltage is less than 0.7 s, which concludes the resonant performance of the bladeless wind turbine.

6. Conclusions

To find a serious solution for expensive renewable energy installations and maintenance such as wind turbines, the authors introduce one of the novel approaches in this scope: the bladeless wind turbine. In this paper, the bladeless wind turbine has been designed, developed, simulated, and tested. The design procedures take into consideration the nature of wind power, so a suitable Fluid-Structure Interaction (FSI) module has been created to examine the aerodynamic performance and extract the output reaction forces for the most reliable cross-section which is a circular section. The study after that extended to simulate the Eigen-frequency analysis to feature and durable selection for the bladeless wind turbine materials and dimensions; this analysis mainly aimed to provide tunning state as much as possible during the vortex shedding frequencies bandwidth. Also, the electro-aeroelastic model was developed to simulate the cantilever beam which has an electromagnetic transducer at its tip; therefore, the output power at the wide range of load resistance was investigated and compared with the experimental analysis. As a result, the numerical simulation agrees with the experimental results over a wide range of load resistance. For the coil and magnets used in this study, the maximum output volt that can be harvested from one module of a coil and magnet of the alternator of the bladeless wind turbine is 200 mV.

7. Recommendations

To keep the developments in this promising approach the authors are motivated to continue in enhance all design parameters in the bladeless wind turbine such as: changing the cylindrical shape to conical, using of multi-integrated modules of coils and magnets, and parametric sweep analysis to examine the effects of each design parameter in the performance of the bladeless wind turbine.

References

[1] Pandey, R. K. "*Recent Trends in Thermal Engineering"* Springer, 2020.

[2] Sigil Francis, V. U. :Design and Analysis of Vortex Bladeless Wind Turbine". *Materials Today: Proceedings, 2021.*

[3] BORETTO, M. "*Bladeless Wind Energy*. TORINO: POLITECNICO DI TORINO, 2019

[4] Jiyuan Tu, G.-H. Y. "Chapter e1 - CFD Case Studies", *Computational Fluid Dynamics (Third Edition)*. Elsevier, 2018.

[5] G. De Nayer, M. B. "FSI simulations of wind gusts impacting an air-inflated flexible", *Journal of Fluids and Structures, 2021.*

[6] R. Fernandez-Feria, E. S.-R. "On the feasibility of a flexible foil with passive heave to extract", *Journal of Fluids and Structures,* 2022.

[7] Xugang Hua a, C. W., " Experimental investigation of wind-induced vibrations of main cables for suspension bridges in construction phases" *Journal of Fluids and Structures,* 2019.

[8] Gang Hu a, F. L., "Wind energy harvesting performance of tandem circular cylinders with triangular protrusions", *Journal of Fluids and Structures,* 2019

[9] Khaled S.M. Essa, a. F.," Survey and Assessment of Wind-speed and Windpower in Egypt including Air Density Variation", *Wind Engineering,* 2006.

[10] DUAN Jinlong, a. H., "CFD-Based Numerical Analysis of a Variable Cross-Section Cylinder", *J. Ocean Univ. China (Oceanic and Coastal Sea Research),* 2014.

[11] G. Poulin, E. S., "Generation of electrical energy for portable devices Comparative study of an electromagnetic and a piezoelectric system", *Sensors and Actuators A,* 2004.

[12] Arafa, M. A., "Energy harvesting using a flextensional", *Journal of Intelligent Material Systems,* 2016.

[13] Mohammadreza Gholikhani, S. A, " Electromagnetic Energy Harvesting Technology: Key to Sustainability in Transportation Systems", *Sustainability,*2019.

[14] D.Djairam., " *The Electrostatic Wind Energy Converter",* Ph D, Thesis, 2008.

[15] Mahadik, J. S., "Piezoelectric wind energy harvester for low-power sensors", *Journal of Intelligent Material System,* 2011.

[16] Malik, M. A. " Multimodal piezoelectric wind energy harvester for aerospace applications", *International journal of energy research, Wiley,*

2022.

[17] Bruce R. Munson, D. F.," *Fundamentals of fluid mechanics",* Wiley, 2009.

[18] MK Hossain, M. C. " Enhanced mechanical properties of carbon fiber/epoxy composites by incorporating XD-grade carbon nanotube", *Journal of Composite Materials,* 2014.

[19] Prasanna Kumar Ilankeeran, P. M. " Axial Tensile Testing of Single Fibres", *Modern Mechanical Engineering,* 2012

[20] M. Musharraf, I. U. khan, N. khan. "Design of an Oscillating Coil Pendulum energy generating system", *Precedia Computer Science,* 32 639-646, 2014.

[21] Inman, D. J. "*Engineering Vibration (3rd Edition)",* 2013.